Document downloaded from:

http://hdl.handle.net/10251/84325

This paper must be cited as:

Del Río García, AI.; García-Albert, C.; Molina Puerto, J.; Fernández Sáez, J.; Bonastre Cano, JA.; Cases Iborra, FJ. (2017). On the behavior of reduced graphene oxide based electrodes coated with dispersed platinum by alternate current methods in the electrochemical degradation of reactive dyes. Chemosphere. 183:242-251. doi:10.1016/j.chemosphere.2017.05.121.

The final publication is available at

http://dx.doi.org/10.1016/j.chemosphere.2017.05.121

Copyright Elsevier

Additional Information

*Revised manuscript with no changes marked
Click here to view linked References

On the behavior of reduced graphene oxide based electrodes coated with dispersed platinum by alternate current methods in the electrochemical degradation of reactive dyes

*A.I. del Río, C. García, J. Molina, J. Fernández, J. Bonastre, F. Cases **

Departamento de Ingeniería Textil y Papelera, Escuela Politécnica Superior de Alcoy, Universitat Politècnica de València. Plaza Ferrándiz y Carbonell, s/n, 03801, Alcoy, Spain.

Abstract

The electrochemical behavior of different carbon-based electrodes with and without nanoparticles of platinum electrochemically dispersed on their surface has been studied. Among others, reduced graphene oxide based electrodes was used to determine the best conditions for the decolorization/ degradation of the reactive dye C.I. Reactive Orange 4 in sulfuric medium. Firstly, the electrochemical behavior was evaluated by cyclic voltammetry. Secondly, different electrolyses were performed using two cell configurations: cell with anodic and cathodic compartments separated (divided configuration) and without any separation (undivided configuration). The best results were obtained when reduced graphene oxide based anodes were used. The degree of decolorization was monitored by spectroscopic methods and high performance liquid chromatography. It was found that all of them followed pseudo-first order kinetics. When reduced graphene oxide-based electrodes coated with dispersed platinum by alternate current methods electrodes were used, the lowest energy consumption and the higher decolorization kinetics rate were obtained.

Scanning Electronic Microscopy was used to observe the morphological surface differences.

Keywords: reduced graphene oxide; dispersed platinum; alternate current methods; reactive dye; electrochemical treatment.

** To whom correspondence should be addressed.*

Telephone: +34.96.652.84.12

Fax: +34.96.652.84.38

e-mail: fjcases@txp.upv.es (F. Cases)

1. Introduction

In 2010 the Nobel Prize in Physics was granted to Andre Geim and Konstantin Novoselov, not for the discovery of graphene, but for the "groundbreaking experiments regarding the two-dimensional material, graphene" (Nobel Prize Official Web, 2010), based on their study published in 2004 (Novoselov et al., 2004).

Graphene exhibits a theoretical surface area of 2630 $m^2 g^{-1}$, which is much greater than that of graphite (~10 $m^2 g^{-1}$) and even that of carbon nanotubes (1315 $m^2 g^{-1}$) (Pumera et al., 2009). Moreover, the electrical conductivity of graphene is excellent.

Several synthetic methods have been established to prepare graphene, but each one of them, besides possessing different scalability, generates graphene with very different characteristics, which strongly influences the resulting properties. Electrochemical methods represent an interesting approach, since they can be easily

controlled, can be performed under ambient conditions, do not require toxic or dangerous chemical agents (the only reactive used is the electron), and require only simple instrumentation. In this case, the limitations of electrochemical methods are that the electrode or sample where the reduction takes place must be conductive, be electrochemically active and be in contact with the solution. In literature, electrochemically reduced graphene oxide (RGO) has been obtained on different electrode materials such as glassy carbon (Chen et al., 2011; Hilder et al., 2011; Bonanni and Pumera, 2012), gold (Hilder et al., 2011; Bonanni and Pumera, 2012; Sheng et al., 2012), indium tin oxide (ITO) (Hilder et al., 2011) or Pt (Bonanni and Pumera, 2012).

Moreover, due to their high surface area, these electrodes can be used as a support with anchoring sites for metal nanoparticles such as Pt nanoparticles, to produce graphene-nanoparticle hybrids. This combination lead to materials which have enhanced electrocatalytic activity and interesting properties for a variety of applications as methanol oxidation in fuel cells (Zhang et al., 2013; Hsieh, et al., 2013), counter electrodes for dye sensitized solar cells (Yeh et al., 2014), hydrogen gas sensing (Shafiei et al., 2010), oxalic acid sensing (Chen et al., 2013), DNA detection (Yin et al., 2012), among others. In the case of Pt, there is a great dependence of the degradation of pollutants on the presence of chloride. The presence of a relatively small amount of chloride ions seems to inhibit the oxygen evolution reaction (OER), causing an increase of the anode potential. Therefore, there is a higher reactivity of oxychloro compounds and the performance of Pt electrodes can be significantly improved in the presence of NaCl.

Although the dispersion of Pt nanoparticles on graphene surface has been done mainly using chemical methods, currently, electrochemical methods have arisen great interest within the scientific community. As reported in recent studies carried out by our research group (Molina et al., 2014), the synthesis of Pt nanoparticles on the surface of reduced graphene oxide can be accomplished potentiostatically or using alternating current methods such as electrochemical impedance spectroscopy (EIS) technique. With the EIS synthesis technique, a lower effective synthesis time was required to obtain an optimum coating of Pt nanoparticles (Molina et al., 2014).

Considering these previous results, the present work deals with two new approaches in the environmental field. Firstly, the study of the electrochemical behavior of different carbonaceous materials with different structures in solutions containing the dye C.I. Reactive Orange 4, commercially known as Procion Orange MX2R (PMX2R). The carbonaceous materials studied in this part are: glassy carbon (GC), GC with Pt dispersed on its surface (GC-Pt), reduced graphene oxide deposited on a Pt support (RGO) and reduced graphene oxide deposited on a Pt support with Pt dispersed on its surface using a potentiostatic method (RGO-Pt/POT) and a current alternating method (RGO-Pt/EIS). Secondly, considering the voltammetric results as an initial reference for the efficiency of these electrodes, different electrolyses under different conditions were performed to evaluate the degradation and decolorization of PMX2R. In this part, RGO-Pt/POT and RGO-Pt/EIS were studied and later compared to other carbonaceous materials. These materials were activated carbon textile (ACT) and activated carbon textile with Pt dispersed on its surface (ACT-Pt), also studied in previously published works (del Río et al., 2015). In all cases, special attention was paid to the influence of the synthesis method.

The dye selected for these studies, PMX2R, it is a monofunctional reactive dye with a 1, 3, 5-triazinyl group as a functional group and an azo group as chromophore. Reactive dyes are widely employed in the textile industry. However, during the dyeing with reactive dyes, they undergo a secondary reaction consisting on their hydrolysis. These dyes are not easily biodegradable and thus even after extensive treatment, color from unexhausted reactive dyes may still remain in textile wastewater. For this reason, this dye was chosen as a representative model of recalcitrant dyes.

2. Experimental

2.1. Reagents and materials

All reagents used were of analytical grade. For the synthesis: Monolayer graphene oxide (GO) powders were acquired from Nanoinnova Technologies S.L. (Spain). Lithium perchlorate ($LiClO_4$) was purchased from Merck. Pt wires (0.5 mm diameter, 99.99% purity) were acquired from Engelhard-Clal. The area of the electrodes was controlled with Teflon®.

For the characterisation: Sulphuric acid (H_2SO_4), CH_3OH (methanol) and $H_2PtCl_6{\cdot}6H_2O$ (hexachloroplatinic acid hexahydrate) were purchased from Merck. Iron (III) sulfate pentahydrate ($(Fe_2SO_4)_3{\cdot}5H_2O$) was used as received from Acrōs Organics. C.I. Reactive Orange 4 (PMX2R) was purchased from Zeneca. NaCl was from Fluka. When needed, solutions were deoxygenated by bubbling nitrogen (N_2 premier X50S). Ultrapure water was obtained from an Elix 3 Millipore-Milli-Q Advantage A10 system with a resistivity near to 18.2 MΩ·cm.

2.2. Solutions

Voltammetric measurements were performed using the following solutions: 0.5 M H_2SO_4 containing 3.9 g L^{-1} PMX2R and 0.5 M H_2SO_4 as blank solution.

Electrolysis analyses were performed using 0.08 g L^{-1} dye concentrations in 0.5 M H_2SO_4, according to real concentrations in wastewaters (Zaharia and Suteu, 2012). When adding NaCl to the solutions, the concentration was 0.3 g L^{-1}.

2.3. Electrodes. Pretreatment and / or preparation

Pt electrodes were pretreated with a flame treatment to clean their surface according to the method developed by Clavilier (Clavilier, 1979). GC electrodes were also pretreated by polishing the electrode with 1.0, 0.3 and 0.05 μm alumina slurry. For the preparation of ACT electrodes, the company Carbongen S.A. (Spain) supplied a hydrophilic activated carbon fabric (ref HST 1110). To discard the presence of impurities on the surface of the fabric, a previous analysis (not included) by FTIR-ATR was carried out. The ACT electrodes were prepared by cutting strips of 1 cm × 2 cm area from the textile. To ensure a proper electric contact between the textile samples and the 2 mm copper rods used as a support, they were glued (the tip was flattened to improve the electrical contact) using CircuitWorks conductive epoxy resin by Chemtronics. The resin was cured in an oven at 90 °C and wrapped with Teflon tape to protect it from the solution. The dispersion of Pt on GC and ACT electrodes (to obtain GC-Pt and ACT-Pt electrodes) was performed in 5 mM $H_2PtCl_6 \cdot 6H_2O$ and 0.5 M H_2SO_4 aqueous solution by CV from − 0.25 to + 0.4 V at 10 mV s^{-1} during 20 scans with a stainless steel (SS) as counter electrode (CE) and Ag/AgCl (3.5 M KCl) as the reference

electrode. The pretreatment for the CE of SS electrodes was described by del Río et al (del Río et al., 2009a, 2009b).

For the deposition of RGO on the Pt support, GO was reduced on the surface of Pt by CV. The solution used for the synthesis contained ultrapure water, 3 g L^{-1} GO and 0.1 M $LiClO_4$ (supporting electrolyte). A Pt wire was used as CE and working electrode (WE) and Ag/AgCl (3.5 M KCl) was used as reference electrode. To perform the electrochemical synthesis of RGO, the potential was cycled between +0.6 V and -1.4 V at 50 mV s^{-1} for 40 scans. The GO suspension tended to precipitate slowly, reason why bubbling for 3 s with N_2 gas was applied when needed. After the synthesis, the obtained electrodes were rinsed with water and characterized in 0.1 M $LiClO_4$ aqueous solution to observe the characteristic capacitative electrochemical behavior of RGO.

In the electrochemical synthesis of Pt nanoparticles on RGO by the potentiostatic method (from now on called RGO-Pt / POT) the WE was RGO and a Pt wire was used as CE. The reference electrode used was Ag/AgCl (3.5 M KCl). The synthesis solution was 5 mM H_2PtCl_6 in 0.5 M H_2SO_4 at 0 V.

For the synthesis of Pt nanoparticles on RGO using alternating current methods (from now on called RGO-Pt / EIS), the potential from which the measurement started was a potential where Pt synthesis was negligible. This is why +0.4 V (vs. Ag/AgCl 3.5 M KCl) was used. The frequency was 10 Hz and the applied amplitude was ±350 mV (maximum allowed by the equipment). Thus, the potential range during the synthesis varied from + 0.05 V to + 0.75 V.

After the synthesis, the electrodes were characterized by CV in 0.5 M H_2SO_4 to test their characteristic voltammetric response.

Due to the high surface area of ACT and its textile morphology it is very difficult to obtain a representative and reproducible voltammetric response of the species present in the solution. Therefore, the voltammetric response of the dye is poorly detected and overlaps with the ACT response in this medium. Therefore the use of GC electrodes was considered for this characterization. One of the reasons is that it is easy to obtain a reproducible surface after the previous pretreatment which, obviously, allows control of the area. Furthermore, GC electrodes present an appropriate separation between the potential for the oxygen and hydrogen evolution. Assuming these differences between GC and ACT electrodes, the results obtained with GC were only considered to evaluate the range of potentials for oxidation and reduction processes, which were used as reference values in the potentiostatic electrolyses.

2.4. Experimental facilities and equipment

2.4.1. Cyclic voltammetry (CV) and electrochemical impedance spectroscopy (EIS)

An Eco-Chemie Autolab PGSTAT302 potentiostat/galvanostat was used to perform electrochemical measurements using these techniques. In all cases, a three-electrode configuration was used with Ag/AgCl 3.5 M KCl as reference electrode and a scan rate of 50 mV s^{-1}.

2.4.2 Electrolyses

The electrolyses were performed using two different configurations of electrochemical cell (Fig. SM-1). The working conditions for the different experiments carried out are included in table 1. To study oxidation or reduction separately, a divided H-type cell

(divided) was employed. A Nafion 117 (DuPont) cationic membrane was used to separate the compartments. The studies were also carried out with an Eco-Chemie Autolab PGSTAT302 potentiostat/galvanostat at room temperature and constant agitation. When the reduction was performed using ACT as cathode, the anode was a Pt wire. When the oxidation was studied, the anode was ACT-Pt and the cathode was Pt. When the combination of these two processes was studied (oxido-reduction), undivided cell was used (undivided) and the anode was ACT-Pt and the cathode was ACT. In the case of the electrolyses using RGO-Pt electrodes, these were always the anode. When studying only the oxidation, the cathode was a Pt wire. For the oxido-reduction, the cathode was ACT. The reference electrode was Ag/AgCl (KCl 3.5M) in all cases. Moreover, when the H-type cell was used, the non-studied compartment was filled with 0.5 M H_2SO_4 and 0.3 g L^{-1} NaCl. The working volume was 0.055 dm3 and different samples were collected during the electrolyses. The intensity, the charge, the potential difference and the electrode potential in blank solution compartment were also measured.

2.5. Analyses and instruments

Chromatographic analyses were performed by means of High Performance Liquid Chromatography (HPLC) with a Hitachi Elite Lachrom Chromatographic System equipped with diode array detector. The chromatographic separations were performed on a Lichrospher 100RP-18C column (5 µm packing). The method used is that described by del Río et al (del Río et al. 2009b). The detection wavelength (λ_{det}) was set at 486 nm. UV-Visible spectra were also obtained with this system. This was made possible by changing the column for a tubular piece (without any packing inside).

This allowed the sample to flow to the detector with low volume consumption. TOC and TN measurements were performed using a Shimadzu TOC-VCSN analyzer based on the combustion-infrared method. The instrument operated at 720 °C and 20 µL sample injection with an air (free of CO_2) flow rate of 150 mL min^{-1}.

A Jeol JSM-6300 field emission scanning electron microscope was used to observe the morphology of the samples. FESEM analyses were performed using an acceleration voltage of 3 kV.

The FTIR-ATR spectra were recorded with a FTIR NICOLET 6700 spectrophotometer equipped with an ATR device, in which the bottom of the surface prism (ZnSe) serves as the cavity for aqueous samples. The subtraction of the background signal (aqueous solution 0.5 M H_2SO_4) was required to obtain the spectra of the different samples. The spectra were collected at 8 cm^{-1} resolution as a result of an average of 400 scans.

2.6. Electrical Energy per order (EEO):

The calculus of EEO was chosen according to the report of Bolton et al (Bolton et al., 2001), considering that the concentration of pollutants in all cases were low. This parameter is defined as the electrical energy in kilowatt-hour (kWh) required to degrade a contaminant by one of magnitude in a unit of volume (e.g. 1 m^{-3}) of contaminated water or air. The corresponding equation (Eq. 1) is the following:

$$EEO = \frac{\mathrm{P} \cdot \mathrm{t} \cdot 10^3}{\mathrm{V} \cdot \log\left(\frac{A_i}{A_f}\right)} \qquad (1)$$

Where: P is the electric power (kW), t is the time of electrolysis (h), V is the volume treated (m^3), A_i and A_f are the initial and final area of the chromatographic peak associated to the pollutant of interest. In this case the factor of 10^3 converts L to m^3.

In the present study, the values of the dye concentration (g L^{-1}) remaining in solution after the electrolyses were difficult to measure since the percentages of dye degradation were very high. However, the chromatographic peak associated with the chromophore group of the dye (absorbing at 486 nm) could be considered. This is because the area of the peak is directly proportional to the concentration of dye whose chromophore group has not been degraded yet, as previously mentioned. Therefore, the area of this peak was used in calculus instead of concentration.

Even so, the area of the chromatographic peak associated with the dye was difficult to measure in some cases due to the high percentages of decolorization obtained after 24 h of electrolysis and the detection limitations of the equipment. For this reason, a percentage of decolorization of 80 % was considered as a reference value to calculate the EEO consumption. At that point of the electrolysis all the solutions studied gave chromatograms where the peak at 486 nm was still detected, although it is considerably smaller than that of the initial solution. The values obtained have been included in Table 1.

3. Results and discussion

3.1. Voltammetric assays

The electrochemical behavior of RGO, RGO-Pt/POT and RGO-Pt/EIS electrodes was compared to observe the influence of the method used to disperse Pt on the RGO surface. Fig. 1a shows the cyclic voltammograms of RGO and RGO-Pt/POT when cycling

between -0.2 V and + 0.7 V in 0.5 M H_2SO_4. As can be seen, the RGO-Pt/POT electrode showed the characteristic peaks of Pt in this medium. According to the figure inset in Fig. 1a, the electroactivity of RGO electrode was not relevant since the voltammetric charge was two orders of magnitude lower, showing the corresponding capacitative response of the RGO surface (Sheng et al., 2012). However, the oxidation and reduction processes of the underneath support of Pt could be observed probably due to a partial covering with RGO (Molina et al., 2014).

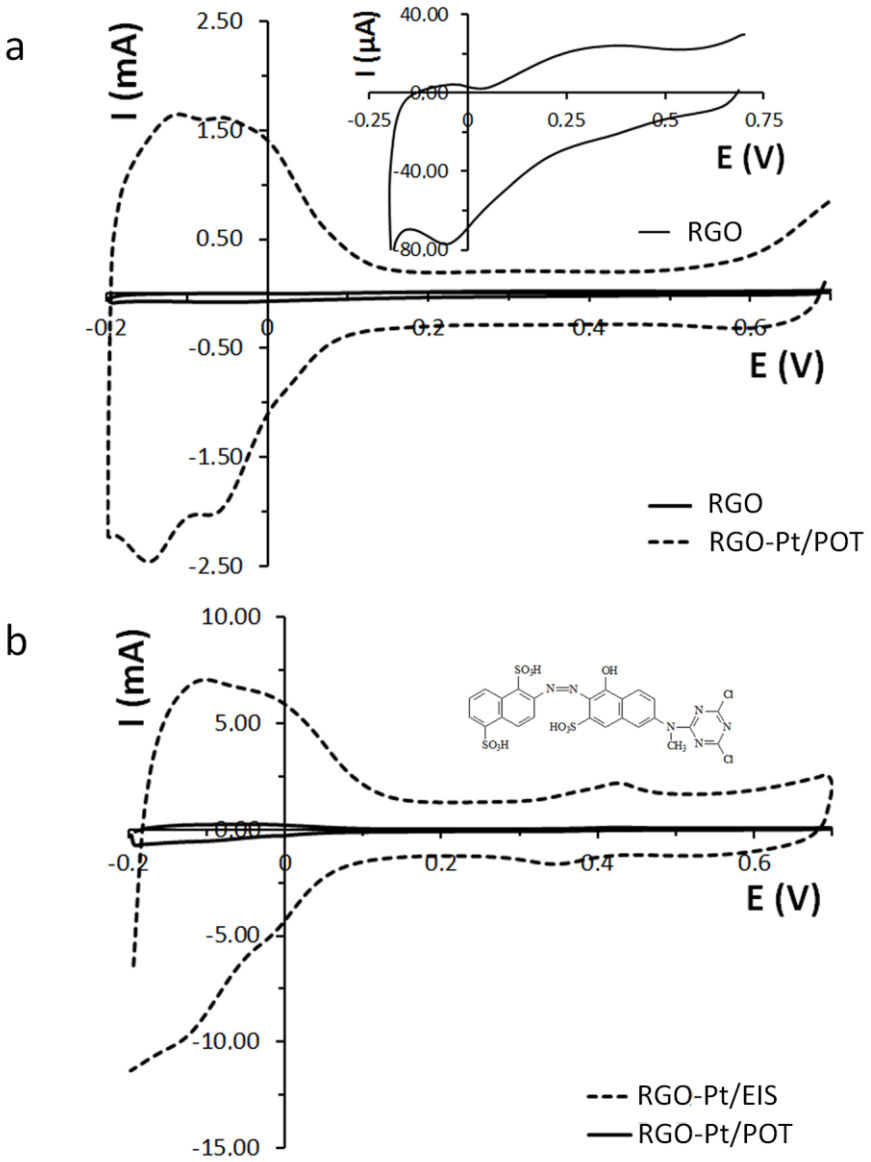

Figure 1. a) Cyclic voltammograms of RGO and RGO-Pt/POT as WE in 0.5 M H_2SO_4. Inset figure: RGO as WE. b) Cyclic voltammograms of RGO-Pt/EIS and RGO-Pt/POT as WE in 0.5 M H_2SO_4 and 3.9 g L^{-1} PMX2R. Inset figure: Chemical structure of C.I. Reactive Orange 4. Second scan in all cases.

This work is mainly focused on the study of RGO-Pt/EIS. However, the study of RGO-Pt/POT electrodes should be considered in order to evaluate the differences and their efficiency. Fig. 1b shows their cyclic voltammograms in 0.5 M H2SO4 and 3.9 g L^{-1} of PMX2R. The RGO-Pt/EIS electrode presents a better electrochemical behavior due to a high number of active sites in Pt covering. This is in accordance with previously published studies (Molina et al., 2014).

To verify this enhancement of the dispersion of Pt nanoparticles by alternate current methods and its influence in the voltammetric behavior of PMX2R, the voltammetric profile of RGO-Pt/EIS electrodes were compared to Pt, GC and GC-Pt electrodes in a 0.5 M H_2SO_4 and 3.9 g g L^{-1} of PMX2R (Fig. 2). Fig. 2a compares GC and GC-Pt electrodes. When GC-Pt was used as WE, the voltammogram profile was similar of bare Pt revealing an adequate covering of the GC surface with dispersed Pt. Apart from the typical reversible peaks of the Pt surface, the oxidation and reduction peaks of the dye were also observed. This can be seen when this profile is compared with the inset figure of Fig. 2a that shows the GC and GC-Pt voltammograms obtained in 0.5 M H_2SO_4. The GC-Pt electrode shows higher electroactivity than GC and the presence of Pt on its surface is clearly evident according to the voltammetric profile.

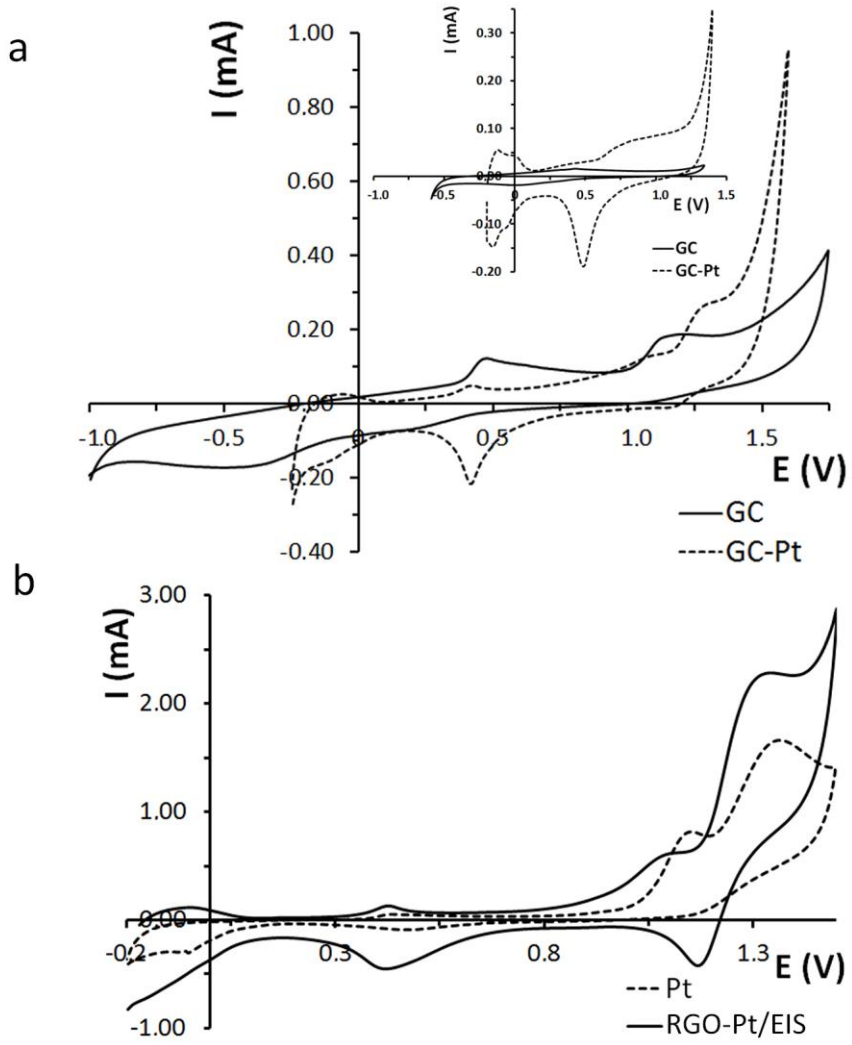

Figure 2. a) Cyclic voltammograms of GC and GC-Pt as WE in 0.5 M H_2SO_4 and 3.9 g L^{-1} PMX2R. Scan rate: 50 mV s^{-1}. Inset: Cyclic voltammograms of GC-Pt and GC as WE in 0.5 M H_2SO_4 solution; scan rate: 10 mV s^{-1}. b) Cyclic voltammograms of Pt and RGO-Pt/EIS as WE in 0.5 M H_2SO_4 and 3.9 g L^{-1} PMX2R solution; scan rate: 50 mV s^{-1}. Second scan in all cases.

Fig. 2b shows the voltammograms of Pt and RGO-Pt/EIS. Both voltammograms present a similar profile. The oxidation and reduction of bare Pt were observed at potential values lower than 0.1 V and higher than 0.5 V. At potential values between + 1.0 V and + 1.50 V, two oxidation peaks are observed. These are attributed to a double contribution of the oxidation of the electrode surface and the oxidation of the dye. The reduction peak observed in the reverse scan at 1.2 V is associated with the

corresponding reduction of the intermediates generated from the dye oxidation. The reduction peak observed approximately at 0.5 V, corresponds to the reduction of Pt oxides. It is worth noting that the charge associated with the electrochemical behavior of RGO-Pt/EIS is significantly higher; indicating that this electrode is clearly more electrocatalytic in these conditions. This can be explained by the higher surface area of RGO. The higher charge of H adsorption (among other processes) on the Pt surface implies a higher electrochemical surface area as result of the small size and uniform dispersion of Pt (Molina et al., 2014). Therefore, more Pt nanoparticles are available to catalyze the electrochemical reaction. In conclusion, the RGO-Pt/EIS electrode is more electroactive than bare Pt with the great advantage that a lower quantity of Pt is needed. Moreover, it is important to highlight that the electroactivity of RGO-Pt/EIS is one order of magnitude higher than in case of using GC or GC-Pt, independently of the presence or absence of dye in solution. In addition to this, it should be noted that GC, GC-Pt and Pt electrodes were chosen as WE in voltammetric assays in order to establish the adequate potentials to carry out the electrolyses where ACT was used as cathode and ACT-Pt and RGO-Pt were used as anodes. Considering their voltammetric behavior in a 0.5 M H_2SO_4 solution containing 3.9 g L^{-1} PMX2R, it was found that the oxidation of the dye takes place at + 1.3 V approximately. The potential needed for the corresponding reduction was located between - 0.1 V (for GC-Pt and Pt) and – 0.4 V (for GC). With the purpose of ensuring the oxidation and reduction processes during the electrolyses, potentials were slightly modified applying cathodic and anodic overpotentials. Therefore, the potentials applied for reduction and oxidation were - 0.35 V and + 1.50 V, respectively.

Since the electrolyses performed in this work were done with solutions containing 0.3 g L^{-1} NaCl, the voltammetric characterization of RGO-Pt/EIS was also studied in this media (Figure not shown). The cyclic voltammogram presented the same profile as in the absence of chloride (Fig. 2-b). However, since chloride ions play an important role in the oxidation, an appreciable difference in the voltammetric charge was observed when chloride is in solution (Trasatti, 1987).

The voltammetric characterization in 0.5 M H_2SO_4 of different RGO-Pt/EIS electrodes obtained at different frequencies has been previously published by our investigation group (Molina et al., 2014; Fig. 8a). According to that study, the most appropriate frequency for the synthesis of Pt on the RGO surface was 10 Hz (the reason why this frequency was chosen for this study). Comparing the voltammogram of RGO-Pt/EIS (at 10 Hz) obtained in 0.5 M H_2SO_4 (Molina et al., 2014; Fig. 8a) and the voltammograms of RGO-Pt/EIS (also at 10 Hz) obtained in 0.5 M H_2SO_4 and 3.9 g L^{-1} PMX2R (Fig. 2b of the present paper,) a considerable diminution of the voltammetric charge was observed in the presence of PMX2R. This can be explained by a partial blockade of the surface due to the dye and/or the intermediates generated and could explain the slight shift observed for the peak associated with the reduction of Pt oxides (Molina et al., 2014; Fig. 8a). Additionally, it is interesting to compare the voltammetric charge when RGO-Pt/EIS was used as WE (Fig. 2b) and when GC and GC-Pt were used as WE (Fig. 2a) in a 0.5 M H_2SO_4 solution and 3.9 g L^{-1} PMX2R. It was found that cyclic voltammograms using GC and GC-Pt as WE presented a voltammetric charge one order of magnitude lower than in case of using RGO-Pt/EIS.

3.2 Electrolyses

3.2.1. Spectroscopic results

Fig. 3 shows the UV-Vis evolution spectra for the processes where a satisfactory decolorization was obtained. Fig. 3b and c (experiments 1 and 2) show that no decolourization was obtained in oxidation and oxido-reduction with ACT-Pt as anode. The spectra of the final samples correspond to 24 h, except Fig. 3g and h (only 4 hours) because of the faster decolorization.

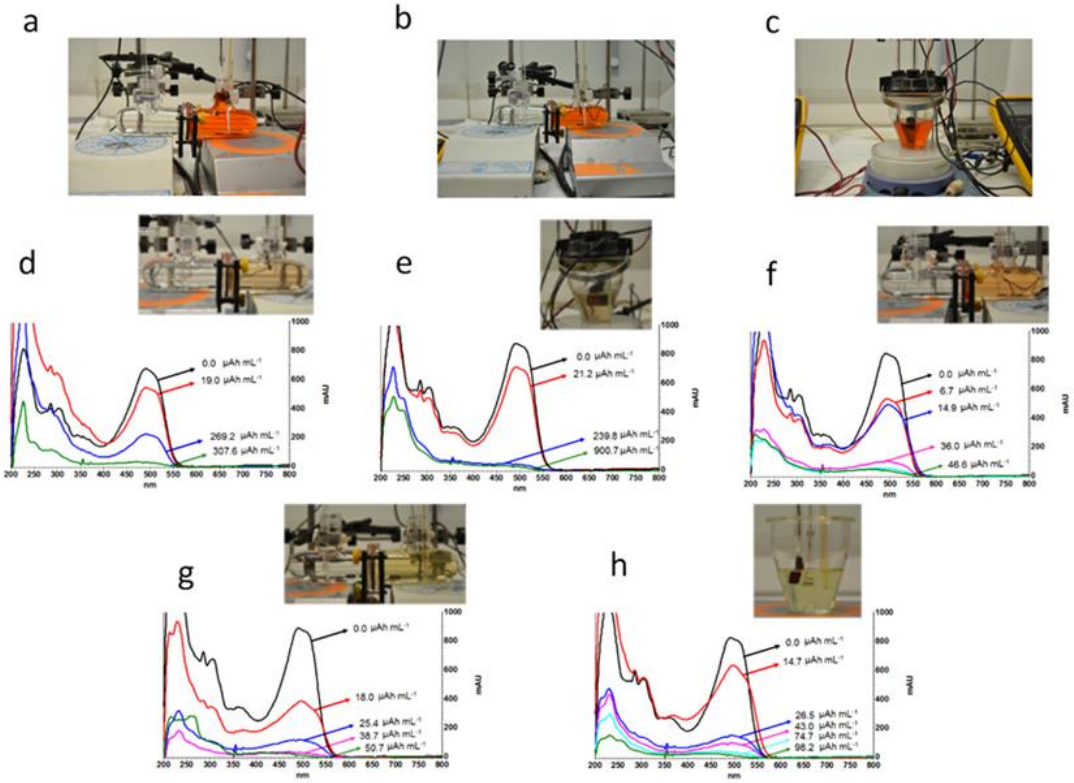

Figure 3. UV-Vis evolutions of 0.08 g L^{-1} PMX2R in 0.5 M H_2SO_4. a) Initial solution. b) Experiment number 1. c) Experiment number 2. d) Experiment number 3. e) Experiment number 4. f) Experiment number 5. g) Experiment number 6. h) Experiment number 7. Inset images: solution after the electrolyses.

The main bands studied were:

- The band at 486 nm, associated with the long conjugated π system linked by the azo group and, therefore, to the decolourization obtained (Silverstein et al., 1991; Lucas and Peres, 2006) as observed in Fig. 3d to h (experiments 3 to 7). The inset image of Fig. 3f shows some color in the final solution suggesting that more than 24 hours are needed for a complete degradation of these bonds.
- The bands at 230 nm and 310 nm, corresponding to π→π* transitions of benzenic and naphthalenic rings, respectively (Yang, 1987; Feng et al., 2000; Galindo et al., 2000; Stylidi et al., 2004). Fig. 3d to h (experiments 3 to 7) show a diminution of these bands indicating a loss of aromaticity, although some benzenic compounds remain in solution (the band at 230 nm does not disappear completely).
- The band at 350 nm, derived from π–π* transition between π system of naphthalenic ring, the -SO_3 groups and the π* system of the –N=N– group (Galindo et al., 2000; Cheninia et al., 2011). As shown in Fig. 3d to h (experiments 3 to 7), naphthalene structures were degraded to give benzenic compounds.
- The band at 280 nm, corresponding to the triazinic group (Silverstein et al., 1991). As observed in Fig. 3d to h (experiments 3 to 7), this structure was completely degraded.
- The band at 245 nm, corresponding to the Ar-NH-NH-Ar' structure (Feng et al., 2000; Qing, 1989). The appearance of this band was only observed in Fig. 3d (experiment 3).

- The band at 260 nm, associated to oxidized benzene compounds (Feng et al., 2000). Fig. 3e to h (experiments 4 to 7) demonstrate the presence of these compounds in solution even after the treatment.

The FTIR-ATR spectra of the samples obtained after the different electrolyses are shown in Fig. 4. The main bands of the original dye (spectrum 0) are:

- Bands at 1050 cm^{-1} (I) and 1192 cm^{-1} (II), ascribed to -SO_3 symmetric and asymmetric stretching vibrations and naphthalene ring deformation (Snehalatha et al., 2008). These bands diminish considerably after the reduction with ACT as cathode (spectrum 3) indicating the structural modifications in the naphthalene groups commented in Fig. 3d and the partial elimination of the -SO_3 groups. After the oxido-reduction with ACT as cathode and ACT-Pt as anode (spectrum 4), the diminution of these bands corroborates the results mentioned in Fig. 3e. The decrease of the band II suggests the oxidation of -SO_3 groups, as indicated in Fig. 3e (band at 260 nm). After the oxidation using ACT-Pt as anode and Pt as cathode (spectrum 1), bands I and II were not observed.
- The band at 1637 cm^{-1} (III), probably corresponding to the imine group (C=N-) of the tautomeric form of PMX2R [30] or to the C-C stretching mode of the naphthalene ring. In spectrum 3 this band appears wider and more intense. This could be related to the bending of the amine N-H bond (Socrates, 1997). This is in accordance with the bands at 245 nm observed in Fig. 3d. In spectrum 4 this band practically disappears due to the partial degradation of the aromatic and chromophore structures. This was also observed in spectrum 1.

- The bands at 1750 cm^{-1} (IV) and 886 cm^{-1} (V), presumably associated with the dichlorotriazine ring (Navarro et al., 1995; Socrates, 1997; Spectral Database for Organic Compounds; Carneiro et al., 2003). In all cases, these bands were not observed confirming the degradation of this group.

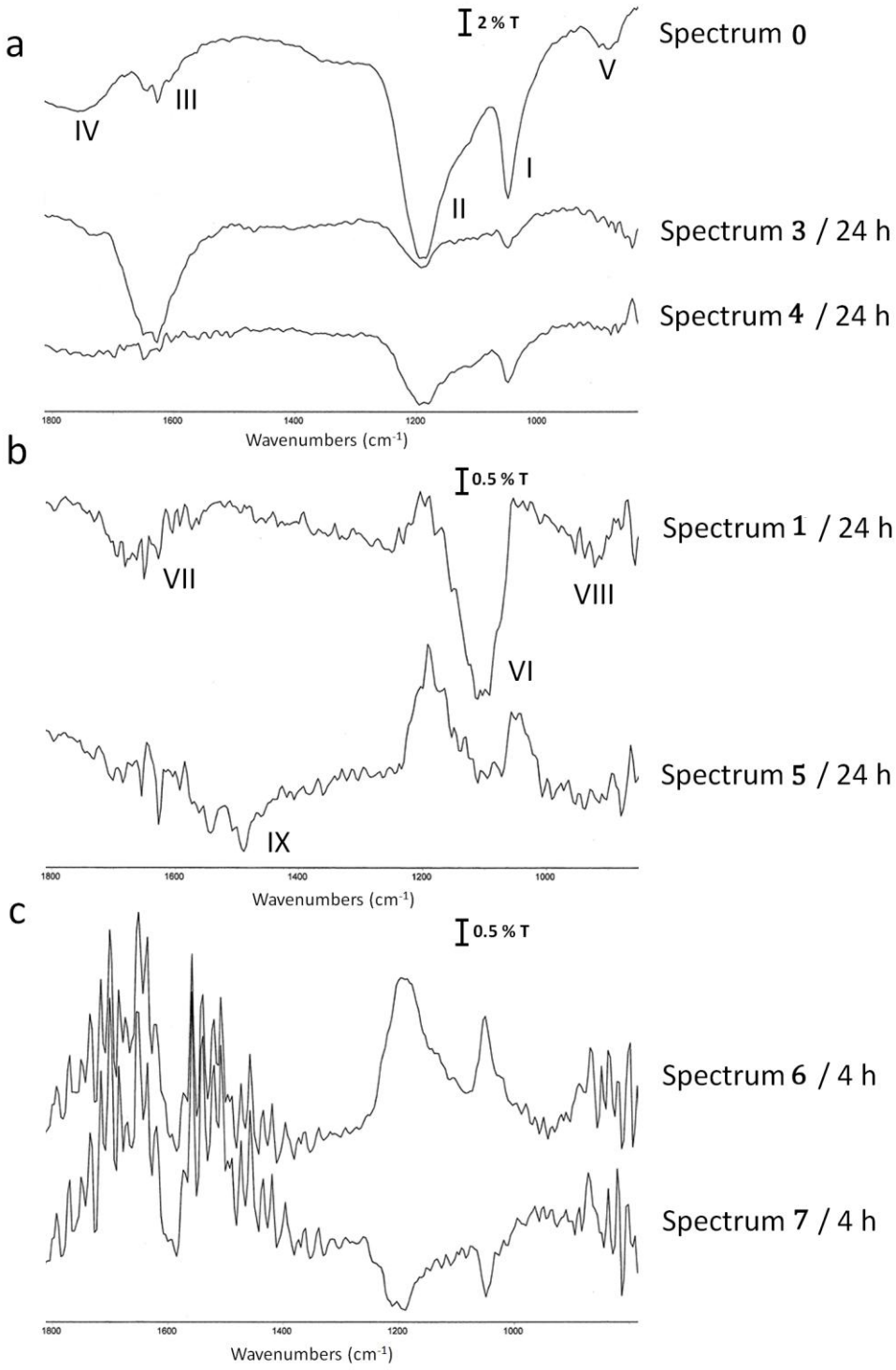

Figure 4. FTIR-ATR spectra of final samples. a) Spectrum 0: initial solution. Spectrum 3: Experiment number 3. Spectrum 4: Experiment number 4. b) Spectrum 1: Experiment number 1. Spectrum 5: Experiment number 5 c) Spectrum 6: Experiment number 6. Spectrum 7: Experiment number 7.

In addition to this, new bands appeared:

- Bands at 1106 cm^{-1} and 1660 cm^{-1} (spectrum 1, VI and VII, respectively), attributed to hydroxyl and carbonyl groups (Carneiro et al., 2003). The band at 1660 cm^{-1}could be also assigned to C=N stretching vibration. This band and the weak band at 930 cm^{-1} (VIII, N-O stretching vibration), could indicate the presence of nitro compounds and oximes (Eq. 2) (Socrates, 1997):

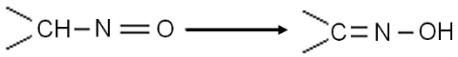

(2)

However, no decolorization was obtained during the oxidation with ACT-Pt as anode maybe because of the appearance of other chromophore structures or a contribution of the band III overlapped with band VII.

After the oxidation and oxido-reduction with RGO-Pt (spectra 5 to 7) all these bands diminished indicating a severe degradation.

- The band centered at 1526 cm^{-1} (IX), probably associated with the asymmetric NO_2 stretching vibration (spectrum 5) (Socrates, 1997).

In samples collected after oxidation and after oxido-reduction with RGO-Pt/EIS (spectra 6 and 7) none of the bands mentioned above were observable after 24 h of

electrolysis. For this reason, the FTIR-ATR spectra shown correspond to samples of solution treated for 4 h.

From these results, Fig. 5 show the reaction mechanisms proposed for electro-reduction and electro-oxidation.

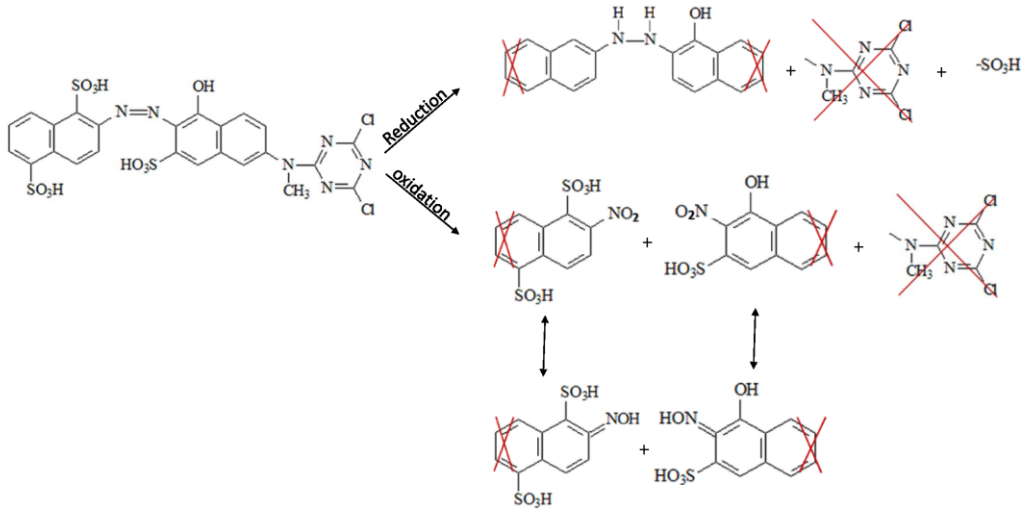

Figure 5. Oxidation and reduction reaction mechanisms.

3.2.2. Kinetics results

Decolorization during the electrolyses was also monitored by means of HPLC technique. With this purpose, the evolution of the dye concentration while passed charge (Q) increased was measured according to the chromatographic area of the peak associated with the dye when the detector wavelength was set at 486 nm. This was possible considering that the dye concentration is directly related to the chromatographic area. Table 1 shows a compilation of the kinetics results obtained from the linear regression analysis for the plots $Ln(A_t/A_o)$ vs. Q ($\mu Ah\ mL^{-1}$) where A_o and A_t are the area of the dye chromatographic peak (at 486 nm) of the initial sample

and the area of a sample taken at t time after electrolysis began, respectively. Table 1 shows, too, the Q needed to obtain a complete decolorization (assuming a decrease in dye concentration of 99 per cent as complete decolorization). All the decolorization processes studied in this work agreed with pseudo-first order kinetics. As can be seen, the ACT electrodes (experience numbers 3-4) presented the slower decolorization rate (see k values in Table 1), independently of the electrochemical cell configuration. In fact, the value of Q necessary to obtain a complete decolorization is 500 – 550 μAh mL^{-1} in both cases.

Table 1. Kinetics analyses obtained for all the electrolyses: decolorization kinetics rate ($\mu A^{-1}\ h^{-1}\ mL$), specific charge (μAh mL^{-1}) for a complete decolorization (99 per cent), percentage of decolorization after 24 h of electrolysis and electrical energy per order (kWh m^{-3}) corresponding to an 80 per cent decolorization.

Experiment number/WE	Cell configuration	WE potential (V)	Electrolyte	k (mL $\mu A^{-1}\ h^{-1}$)	$Q_{decol\ 99\ \%}$ (μAh mL^{-1})	% decol 24 h	$EEO_{decol\ 80\%}$ (kWh m^{-3})
1/ACT-Pt	Divided	1.50	0.5 M H2SO4 + 0.3 g L-1 NaCl	-	-	-	-
2/ACT-Pt	Undivided	1.50	0.5 M H2SO4 + 0.3 g L-1 NaCl	-	-	-	-
3/ACT	Divided	-0.35	0.5 M H_2SO_4	0.0086	535.80 (t > 24 h)	92.88	0.0239
4/ACT	Undivided	-0.35	0.5 M H_2SO_4	0.0116	511.80 (t ≈ 16 h)	100.00	0.0316
5/RGO-Pt/POT	Divided	1.50	0.5 M H_2SO_4 + 0.3 g L^{-1} NaCl	0.0589	77.35 (t > 24 h)	93.81	0.0415
6/RGO-Pt/EIS	Divided	1.50	0.5 M H_2SO_4 + 0.3 g L^{-1} NaCl	0.1800	26.08 (t ≈ 1 h)	100.00	0.0127
7/RGO-Pt/EIS	Undivided	1.50	0.5 M H_2SO_4 + 0.3 g L^{-1} NaCl	0.0608	79.46 (t ≈ 2.8 h)	100.00	0.0564

In the case of RGO-Pt electrodes, the oxidation was more effective when the anode was RGO-Pt/EIS. Actually, the decolorization rate was three times higher than the rate of RGO-Pt/POT electrodes. Moreover, on an equal basis, the electrolyses carried out with RGO-Pt/EIS needed only 26.08 µAh mL^{-1} for a complete decolorization. This means that no more than 1 hour is required for a complete decolorization (this agrees with the spectroscopic results, see Fig. 3) while the value of Q required with RGO-Pt/POT electrodes is three times higher and more than 24 hours are needed.

In the oxido-reduction process with RGO-Pt/EIS as anode, the decolorization rate was lower compared with that obtained after the oxidation with the same electrode. Moreover, a higher electrolysis time and charge were required to obtain a complete decolorization.

3.2.3. Electrodes stability

These results show indisputable evidences that the best results were obtained with RGO anodes with platinum dispersed using alternating current method (RGO-Pt/EIS). However, different reasons such as economy, adaptability, availability of the working space, etc. imply to choose the most appropriate combination. Consequently, the stability of RGO-Pt/POT and RGO-Pt/EIS electrodes in divided and undivided configurations were respectively evaluated. Fig. 6 shows the voltammograms registered in 0.5 M H_2SO_4 before and after the electrolyses. Dispersed Pt is still present on the surface of RGO although a small reduction of the number of active sites was detected in both cases. The voltammetric charge obtained with RGO-Pt/POT as WE

was one order of magnitude lower, indicating a higher electroactivity of the RGO-Pt/EIS electrode, even after the electrolysis.

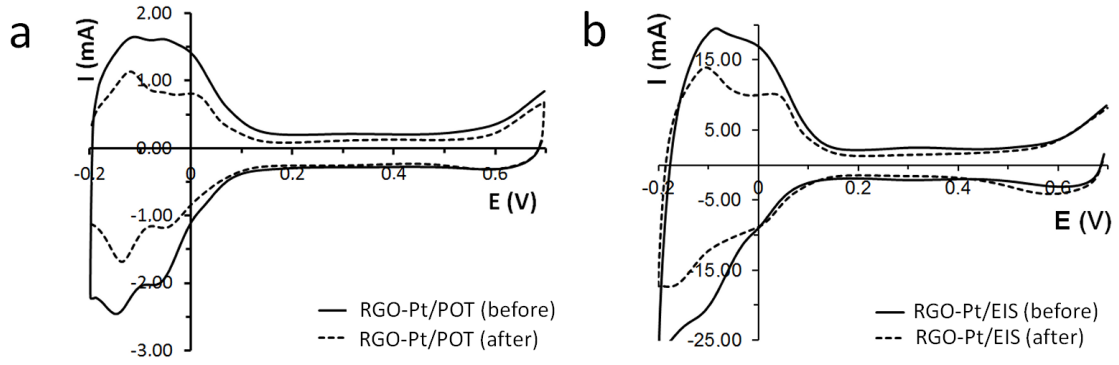

Figure 6. Voltammograms of a) RGO-Pt/POT and b) RGO-Pt/EIS in a 0.5 M H_2SO_4 before and after the electrolysis.

Moreover, the separation between anodic and cathodic peaks of the voltammograms of RGO-Pt/EIS (previously used in the electrolysis of PMX2R) registered in 0.5 M H_2SO_4 and 0.01 M $Fe_2(SO_4)_3$ was 0.085 V, slightly lower than in the case of RGO-Pt/POT (0.092 V) indicating faster electron transfer kinetics (figures not shown).

Fig. SM-2 shows the micrographs corresponding to the coating of a RGO-Pt/EIS anode after performing the electrolysis. As can be seen in Fig. SM-2a, the surface of the electrode showed a very packed coating of dispersed Pt. This reveals a small nanoparticle size and a uniform covering of the RGO surface. After the electrolysis (Fig. SM-2b, the covering showed some cracks although this does not represent a significant influence on the reversibility and the electrocatalytic properties.

3.2.4. Operating costs. Electrical Energy per Order (EEO)

Apart from the kinetics analysis, one of the most important parameters affecting the performance of an electrochemical system is the evaluation of the operating costs.

With this purpose in mind, the electrical energy consumption per order (EEO) was calculated in all cases. The values obtained have been included in Table 1.

From the results in Table 1, the use of RGO-Pt/EIS for the oxidation (divided, experience number 6) required the lowest EEO (kWh m^{-3}). This fact, together with the kinetics results, shows that these are the best conditions to carry out an efficient electrolysis of the PMX2R solution. In addition to this, the trend in EEO values obtained with RGO-Pt electrodes is consistent with the trend of the kinetics results. This means that the higher decolorization rate, the less electrical energy required. However, the use of undivided cell configuration with RGO-Pt/EIS (experience number 7) increased the value of EEO by 77 per cent.

Previous results reported by our research group demonstrated that the RGO-Pt electrode with higher electroactive coating of nanoparticles of Pt was the one obtained by EIS (Molina et al., 2014). Scanning electron microscopy (SEM) provided clear evidence about the coatings obtained in every case. The micrographs revealed that the coating of RGO-Pt/POT electrodes is composed of Pt nanoparticles that are highly ordered and formed as a result of a two-dimensional growth. The size of nanoparticles was found to be very small (Molina et al., 2014; Fig. 6c and d). In the case of RGO-Pt/EIS electrodes, the coating showed three-dimensional growth giving a globular-like structure (Molina et al., 2014; Fig. 6c and d). As a consequence, a greater quantity of Pt nanoparticles is deposited on the RGO surface by EIS and, therefore, a more electroactive coating was obtained.

4. Conclusions

Based on the voltammetric results, the dispersion of Pt on RGO using alternating current method improves significantly the electroactivity of these electrodes since there is a higher number of active sites on their surface in comparison with RGO-Pt/POT electrodes.

It was also found that the degree of decolorization is highly influenced by the cell configuration. The most efficient configuration was the one where anodic and cathodic compartments were separated (divided), which means that there is no relevant synergy between oxidation and later reduction of the dye and intermediates. Moreover, a complete decolorization was obtained in all cases except after the oxidation and the oxido-reduction of C.I. Reactive Orange 4 with ACT-Pt as anode at constant potential of + 1.50 V; although FTIR-ATR studies revealed certain oxidation degree. The rest of the processes showed complete decolorization according to a pseudo-first order kinetics. Spectroscopic results revealed that the hydrogenation of the azo bond is the most probable cause of the decolorization after the reduction with ACT as cathode while the decolorization achieved in the rest of the processes was related to the breakage of the azo bond. Furthermore, the elimination of the triazinic group was shown. The degradation implied a partial elimination of the naphthalene rings to give smaller benzenic compounds that remained in solution and were not eliminated. The best results were obtained when RGO-Pt/EIS electrodes were used with a divided cell, since a complete decolorization was accomplished after 1 h with the lowest electrical energy consumption.

Acknowledgements

The authors wish to thank the Spanish Agencia Estatal de Investigación (AEI) and European Union (FEDER funds) for the financial support (contract MAT2016-77742-C2-1-P). A.I. del Río is grateful to the Spanish Ministerio de Ciencia y Tecnología for her FPI fellowship. J. Molina is grateful to the Conselleria d'Educació, Formació i Ocupació (Generalitat Valenciana) for the Programa VALi+D Postdoctoral Fellowship (APOSTD/2013/056). C. García is grateful to the Conselleria d'Educació, Formació I Ocupació (Generalitat Valenciana) for her Gerónimo Forteza fellowship. The authors wish to acknowledge to Chemviron Carbon who kindly donated the 265 ZORFLEX® activated carbon fabric.

References

Bolton, J.R., Bircher, K.G., Tumas, W., Tolman, C.A., 2001. Figures-of-merit for the technical development and application of advanced oxidation technologies for both electric- and solar-driven systems (IUPAC Technical Report). Pure Appl. Chem. 73, 627–637.

Bonanni, A., Pumera, M., 2012. Electroactivity of graphene oxide on different substrates. Royal Soc. Chem. Adv. 2, 10575–10578.

Carneiro, P.A., Fugivara, C.S., Nogueira, R.F.P., Boralle, N., Zanoni, M.V.B., 2003. A Comparative Study on Chemical and Electrochemical Degradation of Reactive Blue 4 Dye. Port. Electrochim. Acta, 21, 49–67.

Chen, L., Tang, Y., Wang, K., Liu, C., Luo, S., 2011. Direct electrodeposition of reduced graphene oxide on glassy carbon electrode and its electrochemical application. Electrochem. Commun. 13, 133–137.

Chen, X., Cai Z., Huang, Z., Oyama, M., Jiang, Y., Chen, X., 2013. Non-enzymatic oxalic acid sensor using platinum nanoparticles modified ongraphene nanosheets. Nanoscale 5, 5779–5783.

Cheninia, H., Djebbar, K., Zendaouib, S.M. , Sehilia, T., Zouchouneb, B., 2011. Removal of an Azo Dye (Orange G) By Various Methods in Homogenious Phase. Comparative Study. Jordan J. Chem. 6, 307–319.

Clavilier, J., 1979. The role of anion on the electrochemical behaviour of a {111} platinum surface; an unusual splitting of the voltammogram in the hydrogen región. J. Electroanal. Chem. 107, 211–216.

del Río, A.I., Molina, J., Bonastre, J., Cases, F., 2009a. Influence of electrochemical reduction and oxidation processes on the decolourisation and degradation of C.I. Reactive Orange 4 solutions. Chemosphere 75, 1329–1337..

del Río, A.I., Molina, J., Bonastre, J., Cases, F., 2009b. Study of the electrochemical oxidation and reduction of C.I. Reactive Orange 4 in sodium sulphate alkaline solutions. J. Hazard. Mater. 172, 187–195.

del Río, A.I., García, C., Fernández, J., Molina, J., Bonastre, J., Cases, F., 2015. Electrochemical Treatment of Solutions Containing a Recalcitrant Dye: A Way of Using Dimensionally Adaptable Catalytic Fabrics. Ind. Eng. Chem. Res. 54, 6418−6429.

Feng, W., Nansheng, D., Helin, H., 2000. Degradation mechanism of azo dye C. I. reactive red 2 by iron powder reduction and photooxidation in aqueous solution. Chemosphere 41, 1233–1238.

Galindo, C., Jacques, P., Kalt, A., 2000. Photodegradation of the aminoazobenzene acid orange 52 by three advanced oxidation processes: UV/H_2O_2, UV/TiO_2 and VIS/TiO_2: Comparative mechanistic and kinetic investigations. J. Photochem. Photobiol. A: Chem. 130~~(1)~~, 35–47.

Hilde,r M., Winther-Jensen, B., Li D., Forsyth, M., MacFarlane, D.R., 2011. Direct electro-deposition of graphene from aqueous suspensions. Phys. Chem. Chem. Phys. 13, 9187–9193.

Hsieh, S.H., Hsu, M.C., Liu, W.L., Chen, WJ., 2013. Study of Pt catalyst on graphene and its application to fuel cell. Appl. Surf. Sci. 277, 223–230.

Lucas, M.S., Peres, J.A., 2006. Decolorization of the azo dye Reactive Black 5 by Fenton and photo-Fenton oxidation. Dyes and Pigments 71, 236–244.

Molina, J., Fernández, J., del Río, A.I., Bonastre, J., Case,s F., 2014. Synthesis of Pt nanoparticles on electrochemically reduced graphene oxide by potentiostatic and alternate current methods. Mater. Charact. 89, 56–68.

Navarro, A., López González, J.J., Kearley, G.J., Tomkinso,n J., Parker, S.F., Sivia, D.S., 1995. Vibrational analysis of the inelastic neutron scattering spectrum of s-triazine and trichloro-s-triazine. Chem. Phys. 200, 395–403.

Nobel Prize Official Web, 2010. http://www.nobelprize.org/nobel_prizes/physics/laureates/2010.

Novoselov, K.S., Geim, A.K., Morozov, S.V., Jiang, D., Zhang, Y., Dubonos, S.V., Grigorieva, I.V., Firsov, A., 2004. Electric Field Effect in Atomically Thin Carbon Films. Science 306, 666–669.

Pumera, M., Šmid, B., Veltruska, K.J., 2009). Influence of Nitric Acid Treatment of Carbon Nanotubes on Their Physico-Chemical Properties. J. Nanosci. Nanotechnol. 9, 2671–2676.

Qing, C., 1989. Chemistry of Dye Intermediates, Chemical Industry Press, Beijing.

Shafiei, M., Spizzirri, P.G., Arsat ,R., Yu, J., du Plessis, J., Dubin, S., Kane,r R.B., Kalantar-zadeh, K., Wlodarski, W., 2010. Platinum/Graphene Nanosheet/SiC Contacts and Their Application for Hydrogen Gas Sensing. J. Phys. Chem. C 114, 13796–13801.

Sheng, K., Sun, Y., Li, C., Yuan, W., Shi, G., 2012. Ultrahigh-rate supercapacitors based on eletrochemically reduced graphene oxide for ac line-filtering. Sci. Rep. 2, 247.

Silverstein, R.M.C., Basdler, G.C., Morrill, G.C., 1991. Spectrophotometric identification of organic compounds, Wiley; New York.

Snehalatha, M., Ravikumar, C., Sekar, N., Jayakumar, V.S., Hubert Joe I., 2008. FT-Raman, IR and UV-visible spectral investigations and ab initio computations of a nonlinear food dye amaranth. J. Raman Spectrosc, 39, 928–936.

Socrates, G., 1997. Infrared Characteristic Group Frequencies, 3rd ed., John Wiley & Sons, new York.

Spectral Database for Organic Compounds (SDBS), AIST (Japan). http://www.aist.go.jp/index_en.html

Stylid,i M., Kondarides, D.I., Verykios, X.E., 2004. Visible light-induced photocatalytic degradation of Acid Orange 7 in aqueous TiO_2 suspensions. Appl. Catal. B: Environ. 47, 189–201.

Trasatti ,S., 1987. Progress in the understanding of the mechanism of chlorine evolution at oxide electrodes. Electrochim. Acta 32, 369–538.

Yang, J., (1987) Analysis of Dye, Chemical Industry Press, Beijing Ed.

Yeh, M.H., Lin, L.Y., Su, J.S., Leu, Y.A., Vittal, R., Sun, C.L., Ho, KC., 2014. Nanocomposite Graphene/Pt Electrocatalyst as Economical Counter Electrode for Dye-Sensitized Solar Cells. ChemElectroChem 1, 416–425.

Yin, Z., He, Q., Huang, X., Zhang, J., Wu, S., Chen, P., Lu, G., Chen, P., Zhang, Q., Yan, Q., Zang, H., 2012. Real-time DNA detection using Pt nanoparticle-decorated reduced graphene oxide field-effect transistors. Nanoscale 4, 293–297.

Zaharia, C., Suteu, D., 2012. in:Textile Organic Dyes – Characteristics, Polluting Effects and Separation/Elimination Procedures from Industrial Effluentes-A Critical Overview in Organic Pollutants Ten Years After the Stockholm Convention – Environmental and Analytical Update, InTech, Europe.

Zhang, Y., Liu, C., Min, Y., Qi, X., Ben, X., 2013. The simple preparation of graphene/Pt nanoparticles composites and their electrochemical performance. J. Mater. Sci. Mater. Electron. 24, 3244–3248.

Table 1

Click here to download Table: Table 1 revised.docx

Experiment number/WE	Cell configuration	WE potential (V)	Electrolyte	k (mL μA^{-1} h^{-1})	$Q_{decol\ 99\ \%}$ ($\mu Ah\ mL^{-1}$)	% decol 24 h	$EEO_{decol\ 80\%}$ ($kWh\ m^{-3}$)
1/ACT-Pt	Divided	1.50	0.5 M H2SO4 + 0.3 g L-1 NaCl	-	-	-	-
2/ACT-Pt	Undivided	1.50	0.5 M H2SO4 + 0.3 g L-1 NaCl	-	-	-	-
3/ACT	Divided	-0.35	0.5 M H_2SO_4	0.0086	535.80 (t > 24 h)	92.88	0.0239
4/ACT	Undivided	-0.35	0.5 M H_2SO_4	0.0116	511.80 (t ≈ 16 h)	100.00	0.0316
5/RGO-Pt/POT	Divided	1.50	0.5 M H_2SO_4 + 0.3 g L^{-1} NaCl	0.0589	77.35 (t > 24 h)	93.81	0.0415
6/RGO-Pt/EIS	Divided	1.50	0.5 M H_2SO_4 + 0.3 g L^{-1} NaCl	0.1800	26.08 (t ≈ 1 h)	100.00	0.0127
7/RGO-Pt/EIS	Undivided	1.50	0.5 M H_2SO_4 + 0.3 g L^{-1} NaCl	0.0608	79.46 (t ≈ 2.8 h)	100.00	0.0564

Figure 1

Click here to download high resolution image

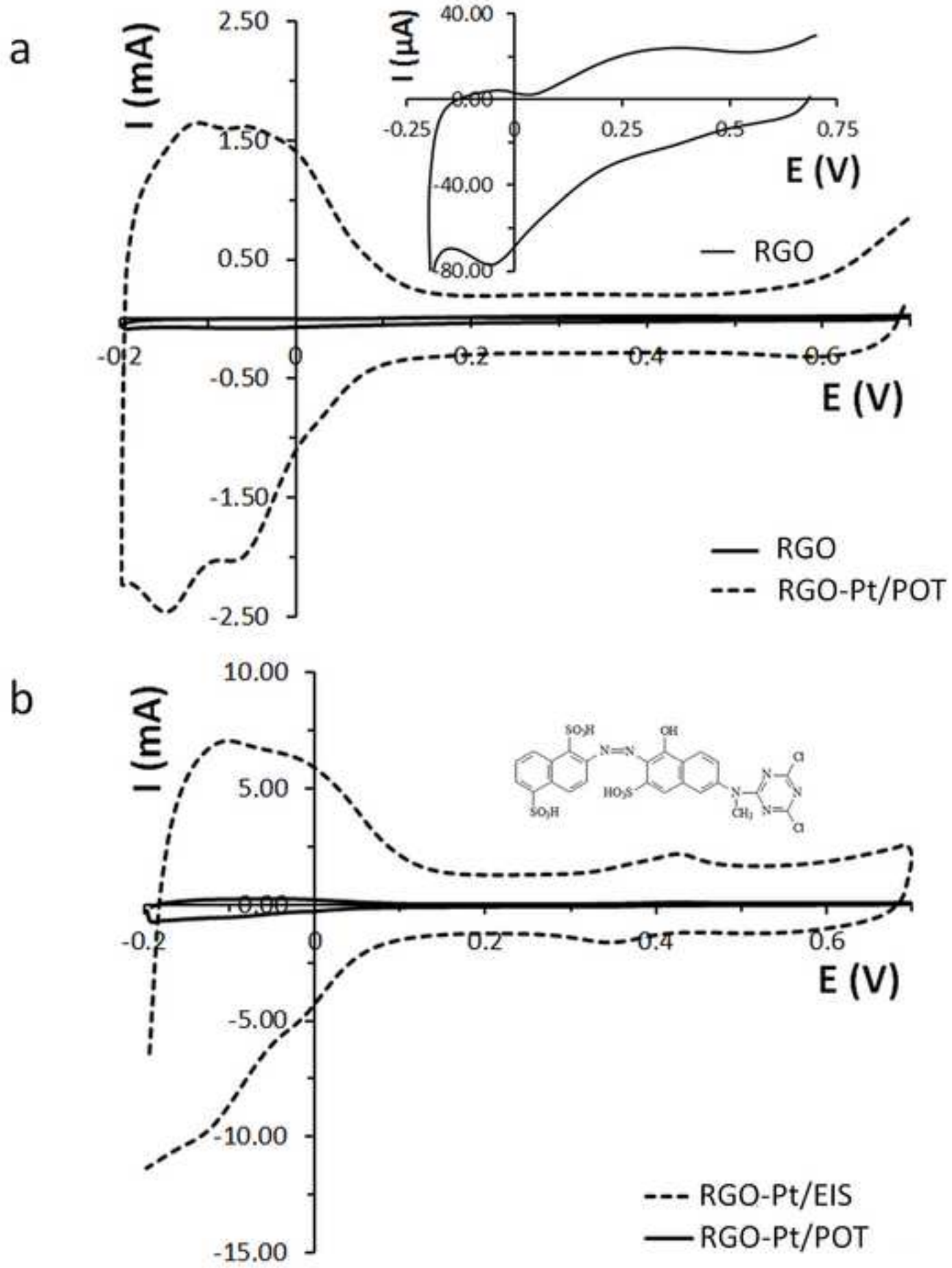

Figure 2
Click here to download high resolution image

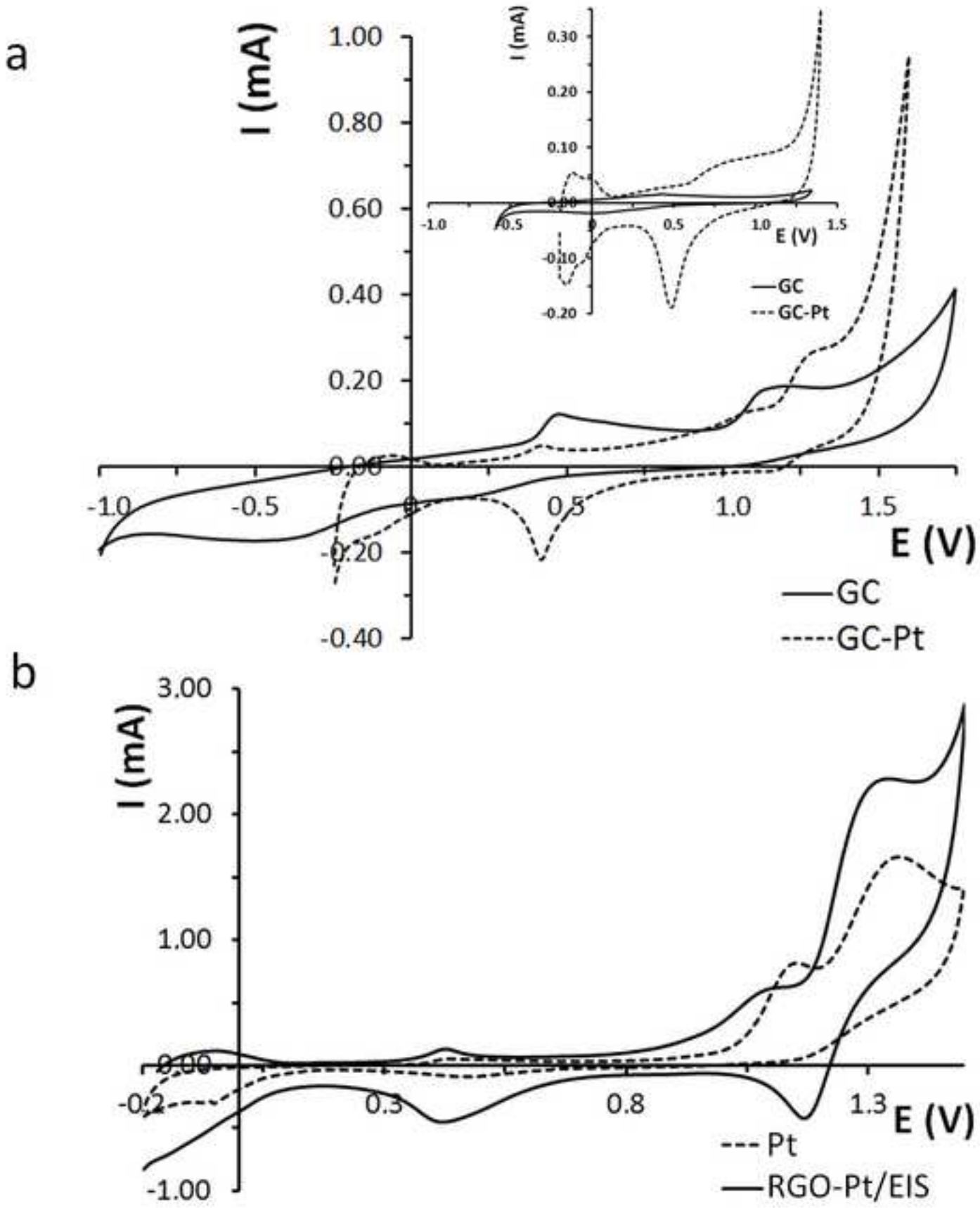

Figure 3

Click here to download high resolution image

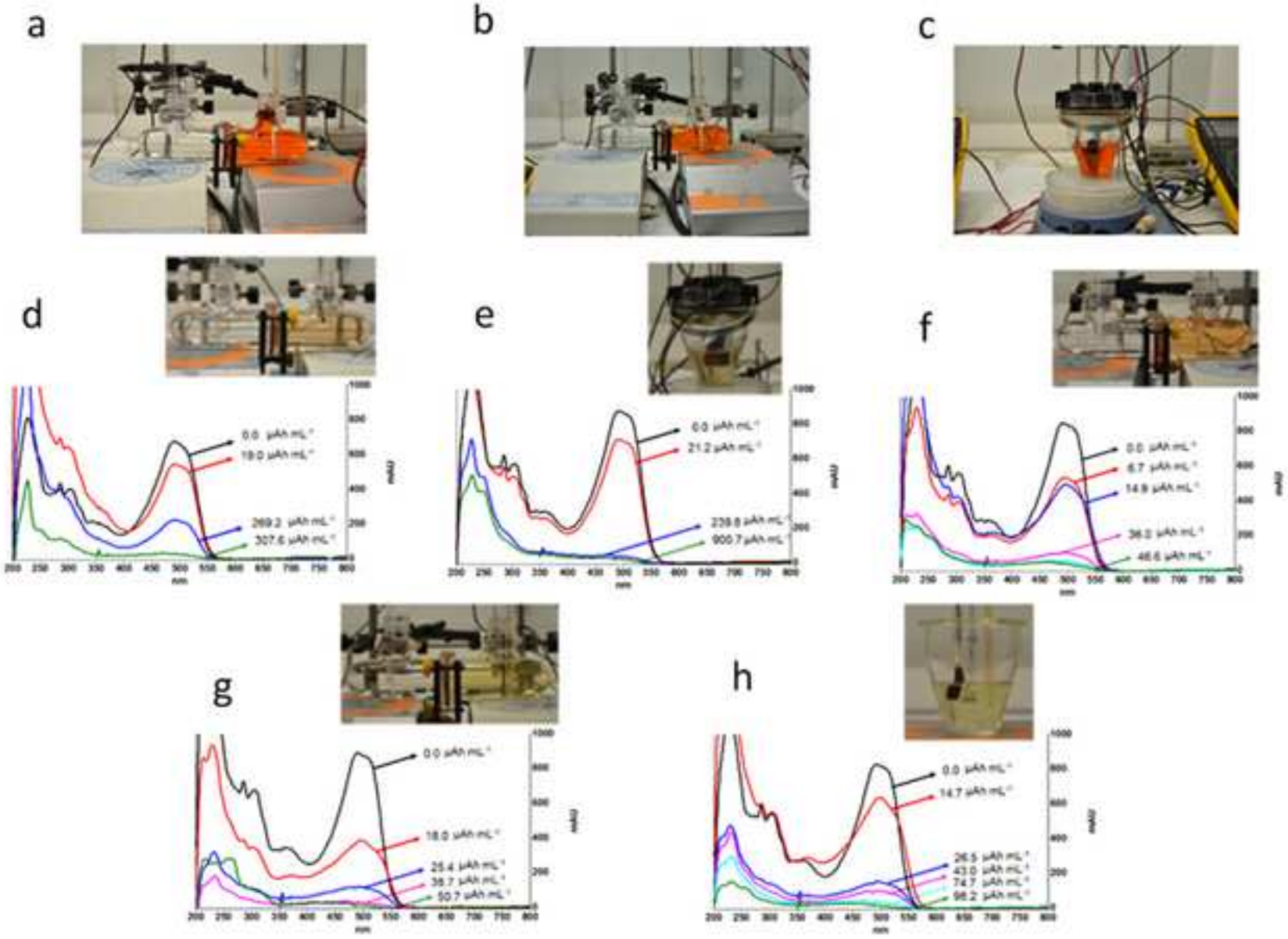

Figure 4

Click here to download high resolution image

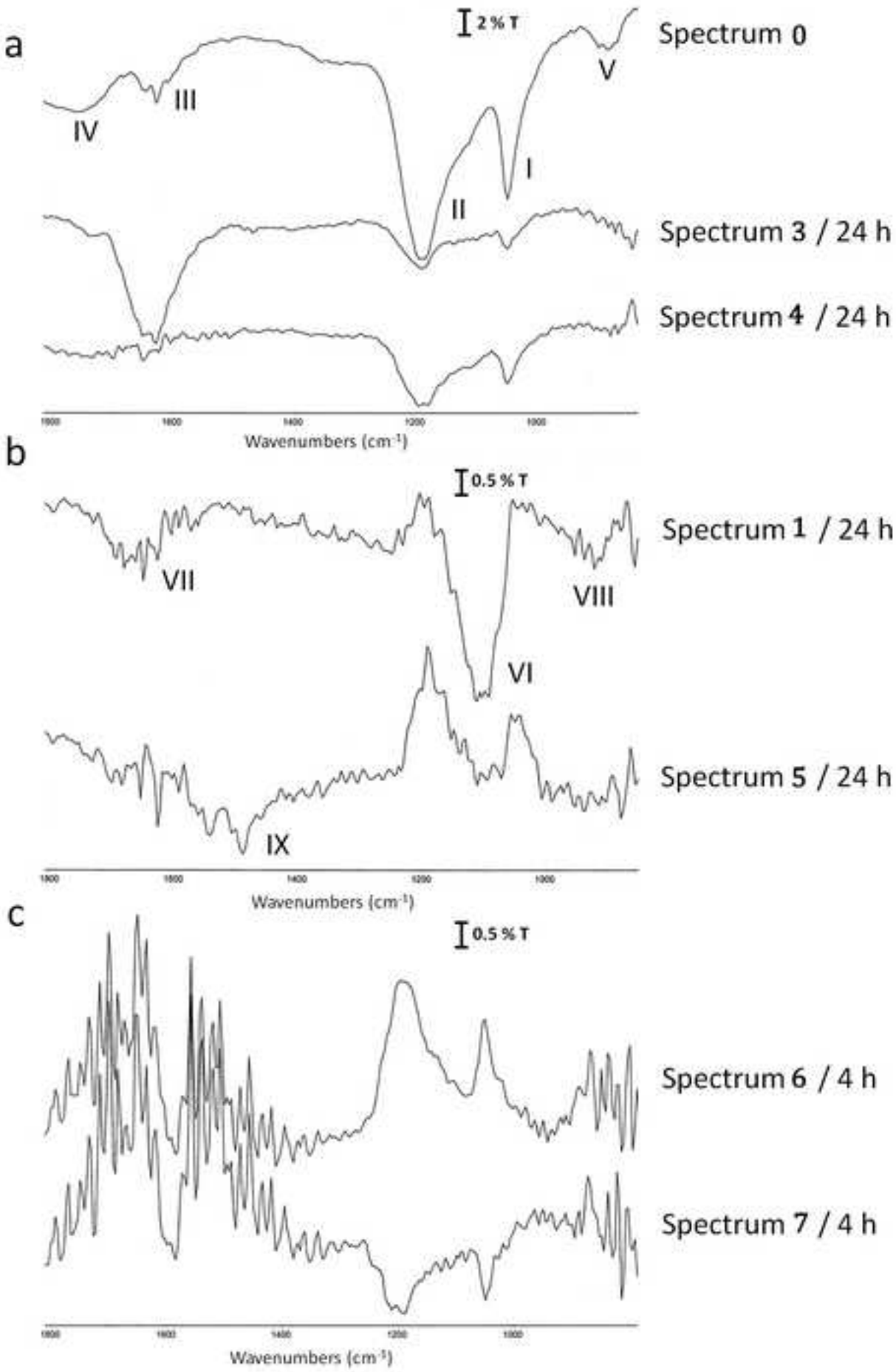

Figure 5

Click here to download high resolution image

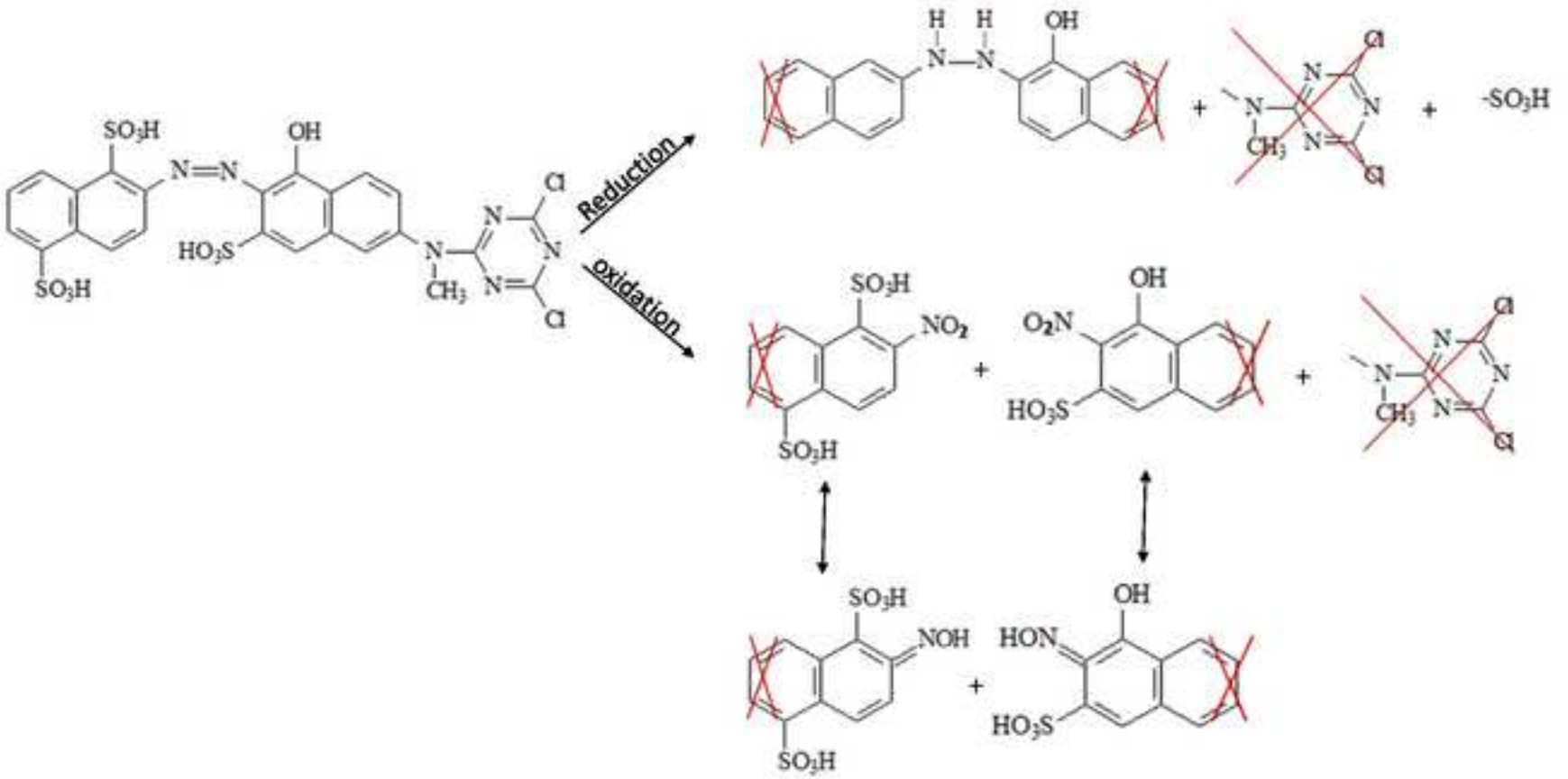

Figure 6

Click here to download high resolution image

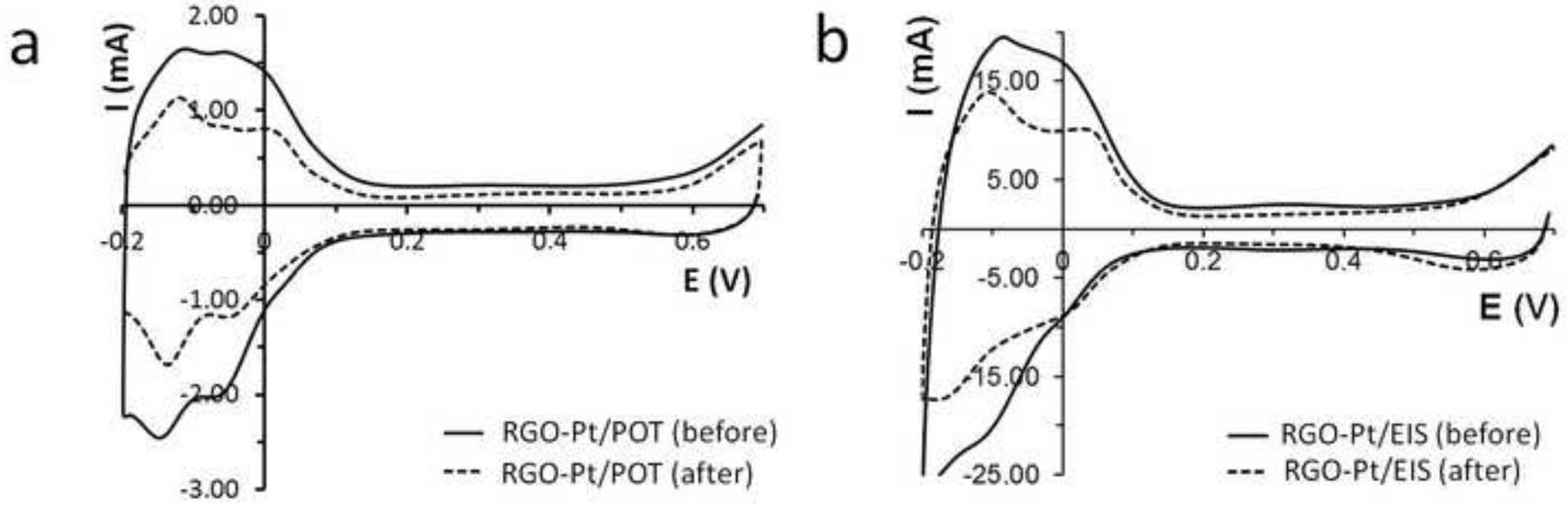

Figure SM-1

Click here to download Supplementary Material: Fig SM-1 revised.tif

Figure SM-2

Click here to download Supplementary Material: Fig SM-2 revised.tif

Table captions

Table 1. Kinetics analyses obtained for all the electrolyses: decolorization kinetics rate ($\mu A^{-1}\ h^{-1}$ mL), specific charge ($\mu Ah\ mL^{-1}$) for a complete decolorization (99 per cent), percentage of decolorization after 24 h of electrolysis and electrical energy per order ($kWh\ m^{-3}$) corresponding to an 80 per cent decolorization.

Figure Captions

Figure 1. Figure 1. a) Cyclic voltammograms of RGO and RGO-Pt/POT as WE in 0.5 M H2SO4. Inset figure: RGO as WE. b) Cyclic voltammograms of RGO-Pt/EIS and RGO-Pt/POT as WE in 0.5 M H2SO4 and 3.9 g L-1 PMX2R. Inset figure: Chemical structure of C.I. Reactive Orange 4. Second scan in all cases.

Figure 2. a) Cyclic voltammograms of GC and GC-Pt as WE in 0.5 M H_2SO_4 and 3.9 g L^{-1} PMX2R. Scan rate: 50 mV s^{-1}. Inset: Cyclic voltammograms of GC-Pt and GC as WE in 0.5 M H_2SO_4 solution; scan rate: 10 mV s^{-1}. b) Cyclic voltammograms of Pt and RGO-Pt/EIS as WE in 0.5 M H_2SO_4 and 3.9 g L^{-1} PMX2R solution; scan rate: 50 mV s^{-1}. Second scan in all cases.

Figure 3. UV-Vis evolutions of 0.08 g L^{-1} PMX2R in 0.5 M H_2SO_4. a) Initial solution. b) Experiment number 1. c) Experiment number 2. d) Experiment number 3. e) Experiment number 4. f) Experiment number 5. g) Experiment number 6. h) Experiment number 7. Inset images: solution after the electrolyses.

Figure 4. FTIR-ATR spectra of final samples. a) Spectrum 0: initial solution. Spectrum 3: Experiment number 3. Spectrum 4: Experiment number 4. b) Spectrum 1: Experiment number 1. Spectrum 5: Experiment number 5 c) Spectrum 6: Experiment number 6. Spectrum 7: Experiment number 7.

Figure 5. Oxidation and reduction reaction mechanisms.

Figure 6. Voltammograms of a) RGO-Pt/POT and b) RGO-Pt/EIS in a 0.5 M H_2SO_4 before and after the electrolysis.

SUPPLEMENTARY MATERIAL

Figure SM-1. Images of the two configuration of the electrolyses cells: a) divided b) undivided.

Figure SM-2. a) FESEM micrograph of a freshly obtained RGO-Pt/EIS electrode. b) FESEM micrograph of RGO-Pt/EIS anode after the electrolysis of a PMX2R solution and 0.3 g L^{-1} NaCl. Anodic potential: + 1.50 V.

Graphical Abstract